Abdul-Aziz, M. K., Nix, A. R., & Fletcher, P. N. (2002). The impact and correction of timing error, frequency offset and phase noise in IEEE 802.11a and ETSI HiperLAN/2. IEEE 55th Vehicular Technology Conference, 2002 (VTC Spring-2002), 1, 214 - 218. 10.1109/VTC.2002.1002695

The Impact and Correction of Timing Error, Frequency Offset and Phase Noise in IEEE 802.11a and ETSI HiperLAN /2

M.K Abdul Aziz, A.R. Nix and P.N. Fletcher

Centre for Communications Research, University of Bristol
Queens Building, University Walk, Bristol BS8 1TR, United Kingdom

Tel: +44 (0)117 954 5169, Fax: +44 (0)117 954 5206
E-mail{M.K.AbdulAziz, Andy.Nix, Paul.Fletcher}@bristol.ac.uk

Abstract *- The aim of this paper is to discuss and explore the impact of practical impairments such as timing error, frequency offset and phase noise on the physical layer performance of IEEE 802.11a and ETSI HiperLAN/2. Standard compliant correction techniques are identified or developed to exploit the allocated preambles and pilot symbols embedded in these standards. The paper includes physical layer performance results in the presence of each form of degradation. These results are presented in terms of packet error rate and bit error rate versus signal to noise ratio for IEEE/ETSI standard indoor channel models of A and E. The performance gain of the corrected receiver is then compared to that of an unaided device. Results indicate that an acceptable level of performance can be achieved over the full range of practical impairments given careful receiver design.*

I. INTRODUCTION

IEEE 802.11a and ETSI HiperLAN/2 represent two future broadband Wireless LAN standards that utilise Coded Orthogonal Frequency Division Multiplexing (COFDM) as the foundation of their transmission strategy. Both standards aim to be deployed in a wide variety of indoor, and possibly outdoor, environments and have the ability to support user mobility in the network. Possible operating environments are described by the IEEE/ETSI standardised channel models, as summarised in table 1.

Since the exact arrival time of COFDM packets in the receiver is unknown in such dynamic surroundings, a problem with frame and symbol timing offset may arise. Any difference between the local oscillator frequencies in the Access Point (AP) and Mobile Terminal (MT) will also cause a received frequency offset, which is detrimental to network performance [1]. Finally, phase noise present in the radio's front end will result in both a Common Phase Error (CPE) and Inter Carrier Interference (ICI) [2]. Given that all three of these degradations are likely to occur in a practical receiver, it is essential that timing synchronisation, frequency offset correction and CPE removal is performed in the receiver prior to payload demodulation.

Given the physical layer harmonisation in 802.11a and HiperLAN /2, almost identical preambles and pilot symbols have been adopted to combat the above mentioned effects. The preamble in the IEEE 802.11a Physical Layer Convergence Procedure (PLCP) header contains 10 OFDM short symbols and 2 long OFDM symbols for coarse and fine frequency offset estimation. This preamble can also be used for timing synchronisation [3]. For the same reasons the ETSI HiperLAN/2 standard allocates an equal length preamble structure to the IEEE 802.11a in its PHY broadcast burst at the beginning of each MAC frame [4]. Continuous pilot tones are also incorporated into each OFDM symbol in both standards in order to ensure coherent detection robustness against frequency drifts and oscillator phase noise.

Table 1: IEEE/ETSI channel models

Mode	Environment	Average RMS delay spread (ns)
A	Office NLOS	50
B	Open space/Office NLOS	100
C	Large open space NLOS	150
D	Large open space LOS	140
E	Large open space NLOS	250

This paper analyses the degradation caused by timing error, frequency offset and phase noise in an IEEE 802.11a and ETSI HiperLAN/2 receiver. All link level transmissions are assumed to occur in the Down-Link (DL) mode where all results are based on the training structure and payload received at the Mobile Terminal (MT). All impairments are discussed and simulated individually to reflect their isolated effect on performance. For each problem, an effective counter measure is introduced and its performance analysed at both extremes of the expected channel conditions (i.e. in channels 'A' and 'E'). Packet Error Rate (PER) curves are generated to compare the ideal (no impairment in the receiver), unaided and aided receiver performance. All results are based on soft Viterbi decoded PHY bursts sent over a statistically large set of channels utilising PHY layer mode 6 (16-QAM modulated with 3/4-rate encoder). The Packet lengths are determined by a payload of 1500 bytes for IEEE 802.11a and 48 bytes (one long PDU) for ETSI BRAN HIPERLAN/2.

The paper is organised as follows. Section II presents the problem of timing synchronisation and the application of a windowing function as a practical solution. Section III discusses the problem of frequency offset in the standards and the use of coarse and fine frequency offset estimation techniques. Section IV presents the degradation caused by phase noise. Finally, the paper concludes by discussing the performance of the various correction methods.

II. TIMING SYNCHRONISATION

The ETSI HiperLAN/2 MAC protocol is based on dynamic MAC frames that are sent continuously every 2ms. The beginning of each frame is preceded by a Broadcast Burst preamble containing ETSI specified SA, SB and SC modulated data elements. In order to preserve the centralised TDMA structure of the HiperLAN/2 standard, timing synchronisation is required to lock on to the first sample of the Broadcast Channel (BCH) preamble [5]. This is shown in figure 1.

In [7] several methods for frame detection were presented using the SA and SB preambles in HiperLAN/2.

0-7803-7484-3/02/$17.00 ©2002 IEEE.

In particular, a time synchronisation algorithm was proposed based on the A and B autocorrelation. In [8], time synchronisation was achieved more accurately by exploiting the double length SC preamble. This approach offers the best resilience in the presence of noise and improves robustness against excessively long delay spread channels. Note that the smallest addressable granularity of these points are given by slots of 400ns.

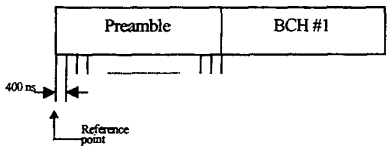

Figure 1 – Sample synchronisation performed in the first broadcast burst after frame detection

In a similar manner, timing synchronisation can be established in 802.11a by using the double-length training symbol (equivalent to the HiperLAN/2 SC preamble) present in the PLCP preamble. In the case of 802.11a case, timing synchronisation is required every time it receives payload from the AP. To achieve optimal performance and ensure 802.11a and HiperLAN/2 compatibility, our time synchronisation is performed using the double-length training preamble.

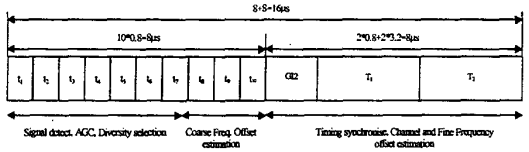

(a) PLCP Preamble for IEEE 802a

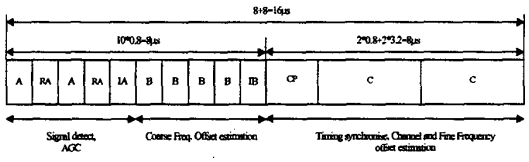

(b) Broadcast Burst Preamble for ETSI HiperLAN/2

Figure 2 - 802.11a and HiperLAN/2 preambles

The method presented here utilises a "windowing method" on the autocorrelation values acquired from the SC preamble. An 800ns window slides across the autocorrelation period of 3.2μs (the unextended symbol period). The final timing is dependent on the maximum value given by $R'_{yy}(\tau')$. The correlator output is given as:

$$R_{yy}(\tau) = \frac{1}{K_{corr}} \int_{t=-1600ns}^{1600ns} y_c(t)\hat{y}_c^*(t-\tau)dt \quad (1)$$

where $\hat{y}_c(t)$ and $\hat{y}_c^*(t-\tau)$ represent the original and conjugate delayed version of the received signal. The integrator output is given as:

$$R'_{yy}(\tau') = \frac{1}{K_{\text{int}}} \int_{\tau=0ns}^{800ns} R_{yy}(\tau-\tau')d\tau \quad (2)$$

where K represents a constant to normalise the windowed energy to a maximum values of one. The peak of this curve corresponds to the point where the desired signal is at its greatest. However, the actual timing point can be chosen at a number of different points since the symbol energy is spread over a relatively wide window (especially for channel model 'A'). This timing window occurs due to the use of a guard interval in OFDM systems. If the delay spread and filter group delay do not span the entire guard interval then any remaining guard can be used to ease the required symbol timing accuracy. Since channel 'A' has the lowest delay spread, it follows that it results in the largest timing window. This can be seen in the results of figure 3, where the energy spread resulting from equation 2 is shown together with the BER resulting from that particular time offset. The BER shows a window of more than 10 samples that result in a minimum error rate. The lowest values of BER correspond well with the largest output from equation 2.

In channel 'E', there is a far greater sensitivity to timing error since delay spread now exceeds the 800ns guard interval. In such a channel, ICI is always inherent in the received OFDM symbols. This characteristic is reflected in figure 4, where the window for optimum timing is far more limited. Once again, the peak of equation 2 can clearly be seen to correspond to the lowest BER. Results are again based on PHY layer mode 6 in a Signal to noise ratio of 18dB.

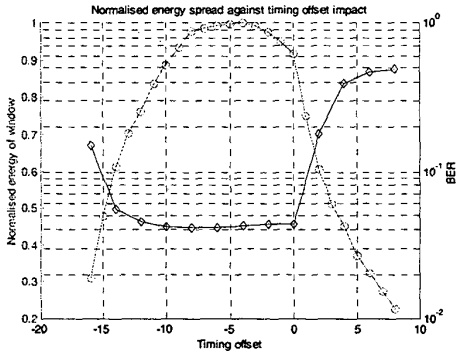

Figure 3 – Normalised Energy versus system BER for ETSI HiperLAN/2 (channel model 'A')

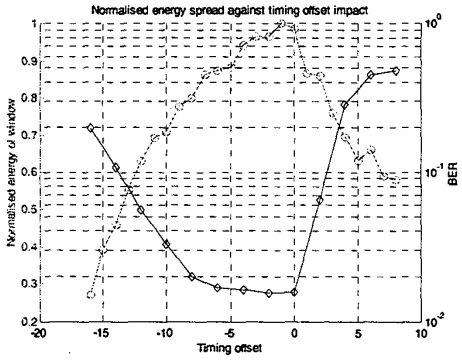

Figure 4 – Normalised Energy versus system BER for ETSI HiperLAN/2 (channel model 'E')

Figure 5 shows the probability density function of the optimum timing point in channels 'A' and 'E' relative to the ideal narrowband case (which has an offset of zero at

the first sample of the payload after the cyclic prefix). These graphs were obtained by simulating the transmission of 1000 preambles over independent uncorrelated fading channels whose expected statistics conform to channel models 'A' and 'E' respectively. An S/N of 10 dB was assumed to ensure the algorithm operates effectively in the presence of noise. For channel 'A' there is a wide spread in optimum timing points. For channel 'E', the larger delay spread ensures a far narrower range of optimum offsets.

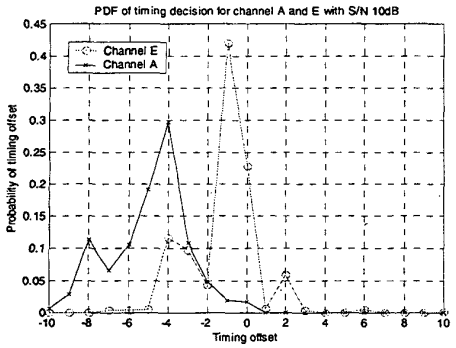

Figure 5 – PDF of "windowing" timing offset over channel models 'A' and 'E' at 10 dB S/N

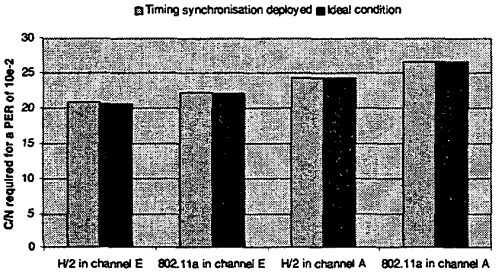

Figure 6 - Comparison of PER performance for ideal (time offset of zero) versus estimated timing recovery.

Figure 6 compares the required signal to noise ratio for a Packet Error Rate (PER) of 1% over channel 'E' using Physical Layer Mode 6. The results show that the performance of the proposed timing algorithm is near identical to the ideal case, even in worst case channel 'E'. 802.11a can be seen to require a higher signal to noise ratio for the same PER. This observation is further discussed in [13].

III. FREQUENCY OFFSET

Both the 802.11a and HiperLAN/2 standards specify a maximum frequency offset per terminal of 20 ppm. Therefore, at an operating frequency of 5.2 GHz, a worst case frequency offset of ±208kHz could be experienced between any two transceivers. The algorithm proposed by Schmidl and Cox [9] enables frequency offsets of up to twice the subcarrier spacing to be corrected (625kHz). However, a problem of standard compliance arises since the technique requires special training symbols which are not supported in the standard. Instead, an algorithm reported by Moose [6] can be used that relies on the transmission of two identical OFDM symbols. Standard compliance is assured since both the SC and PLCP headers fulfil this requirement. However, before applying the Moose algorithm on the SC preamble, a coarse frequency offset correction must be performed to ensure the residual frequency offset lies within ±1/4 of the subcarrier spacing. The coarse frequency offset algorithm exploits the periodic nature of the SB preamble in ETSI HiperLAN/2 and the short training symbols in IEEE 802.11a. The coarse algorithm applies a delay and correlate method as explained in [8] and utilised in [7]. It is reported that the Moose method performs sub-optimally in the presence of very long delay spreads. Here we study the BER performance in channels 'A' and 'E' when applying these coarse and fine frequency offset algorithms in cascade.

$$\bar{f}_{coarse} = \frac{Arg\left(\int_{\tau=0}^{Win_B} \hat{y}_c(t-\tau)\hat{y}_c^*(t-\tau-T)d\tau\right)}{Win_B} \quad (3)$$

Equation 3 is applied pre-FTT to the received time domain waveform of the SB preamble in ETSI HiperLAN/2 or the short training symbol in IEEE 802.11a. The delay T is equal to 800ns and the buffer window period Win_B is 3.2μs. This equation performs coarse frequency offset estimation prior to FFT processing. The resulting output is used to correct the coarse frequency offset thus minimising ICI in the output of the FFT.

$$\bar{f}_{fine} = \left[\frac{1}{2\pi}\right]\tan^{-1}\left(\frac{\sum_{k=-K}^{K} \mathrm{Im}[\,Y_{1,k}Y_{2,k}^*\,]}{\sum_{k=-K}^{K} \mathrm{Re}[\,Y_{1,k}Y_{2,k}^*\,]}\right) \quad (4)$$

Equation 4 computes the fine frequency offset from the FFT outputs for the SC preamble (or double symbol preamble in 802.11a). $Y_{1,k}$ and $Y_{2,k}$ are identical preamble symbols sent of the k-th subband of the first and second OFDM symbol respectively. The value of these subband symbols is quoted in the standards. Any phase variation over these two symbols is assumed to result from a frequency offset. Hence, by averaging the phase offset over all $2K+1$ subbands, an accurate fine frequency offset correction signal can be calculated. This fine error is then used to correct the frequency error prior to payload detection.

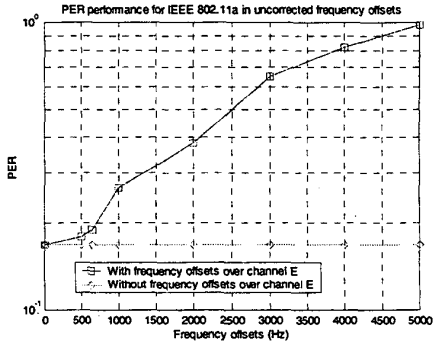

Figure 7 - Effect of uncorrected frequency offset in channel E for 802.11a (S/N of 18dB)

From figure 7 it can be seen that unacceptably high values of PER will result for relatively modest uncorrected

values of frequency offset. For errors of 500Hz and greater, the simulated PER is well in excess of 10%.

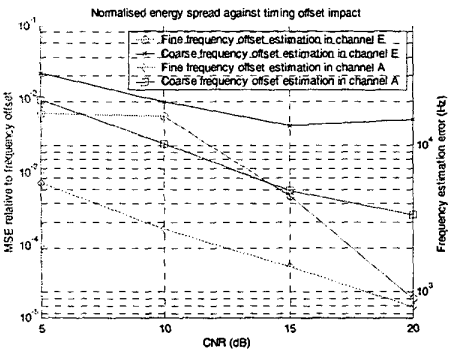

Figure 8 - MSE versus Signal to Noise ratio for a frequency offset of 208kHz over channel E

The MSE is given by:

$$MSE = \frac{1}{T}\int_{t=0}^{T}((f-\bar{f}(t))/f)^2 \partial t \qquad (5)$$

Figure 8 shows that the coarse frequency offset algorithm is able to acquire a suitably accurate frequency offset estimate before applying fine frequency offset estimation. We find that for average signal to noise ratios beyond 15dB, an MSE of 0.004 is achieved for an average frequency offset error of around 13kHz. For fine frequency estimation, at an average signal to noise ratio of 20dB, an MSE of 0.0001 is achieved at an average frequency offset error of around 650Hz.

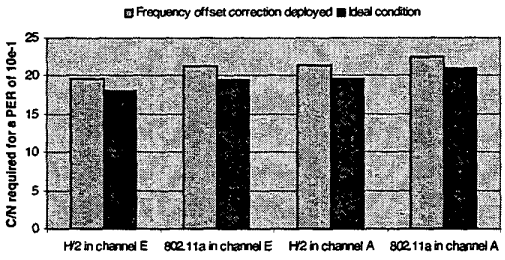

Figure 9 - Comparison of PER performance for Physical layer Mode 6 using coarse and fine frequency offset estimation over Channel A and E

Figure 9 shows that signal to noise ratio degradation resulting from imperfect frequency offset estimation in channels 'A' and 'E'. For channel 'E' the degradation is around 1.6 to 1.8 dB for both standards. In channel A, this degradation is slightly less, at around 1.4 to 1.6 dB.

IV. PHASE NOISE

Although both the 802.11a and HiperLAN/2 standards imposes no specifications to the design criteria of their frequency synthesis components, it is well known that phase noise can be a limiting factor in the OFDM based WLAN standards. Phase noise contributes two degrading factors, namely CPE and ICI [10]. It is known that CPE is correctable and will be the dominating distortion in cases where the phase noise remains relatively stable over an OFDM symbol period (i.e. for a phase noise spectrum where the majority of the power is close in to the carrier frequency). Higher frequency phase noise components cannot be corrected as CPE and result in a loss of subband orthogonality and hence ICI in the received OFDM symbols. Both standards support the use of continuous pilot to enable the application of CPE resulting from low frequency phase noise. Higher frequency phase noise components cannot be corrected and will result in an irreducible error floor.

According to [11], an accurate phase noise model can be generated as the sum of the spectra of all potential contributors to the generation of phase noise. In [13], the phase noise model is represented as a phase modulator cascaded with an amplifier and resonator. The model is given as shown in equation 6.

$$S_{\theta,out}(\Delta f) = \left[1+\left(\frac{f_p}{\Delta f}\right)^2\right] S_{\theta,in}(\Delta f) \qquad (6)$$

where f_p represents the cut-off frequency and is set equal to half the bandwidth of the resonator. $S_{\theta,in}(\Delta f)$ represents the phase modulator transfer characteristic as is determined by the flicker noise which is given as [13]:

$$S_{\theta,in}(\Delta f) = \frac{N_o}{P}\left(1+\frac{f_c}{\Delta f}\right) \qquad (7)$$

where f_c represents the corner frequency of the phase modulator (i.e the start of $\pm$20dB/decade magnitude response) and N_o is the thermal noise power spectral density of the real unity gain amplifier.

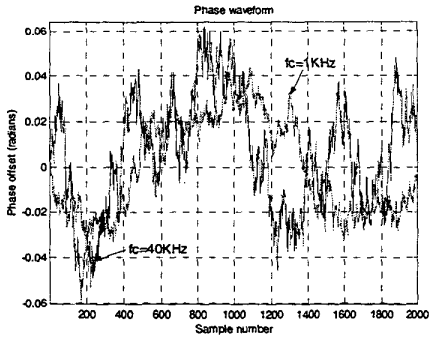

Figure 10 - Phase noise time domain waveforms generated for different corner frequencies

Figure 10 shows that as the corner frequency of the phase modulator rises, the rate of change of phase noise increases. This is hazardous to the frequency offset estimation algorithm since the phase difference would include a random component arising from the phase noise. This impairment is inherent in the received signal regardless of the presence of pilot tones sent over the OFDM symbols, since coarse frequency offset estimation must be applied before the demodulation process. A greater frequency offset error adds to the loss of orthogonality and adds to the ICI terms generated from the phase noise.

Figure 11 presents the constellation diagram for the 64QAM mode (which is most effected by phase noise) in the presence of phase noise but without CPE correction. It shows that the phase noise drifts with time around a zero

mean, resulting in random rotation of the constellation. This result was generated for a corner frequency of 1kHz, a slope [12] of -84 dBc/Hz and a phase noise floor of -132 dBc/Hz. The constellation was plotted over a time period of 100μs. Figure 12 shows that by using the known pilot tones these phase rotations can be corrected. This correction works for CPE since the same phase rotation is applied to all subbands in a given symbol period.

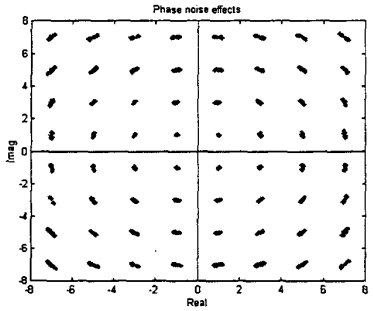

Figure 11 - 64 QAM phase rotation (phase noise)

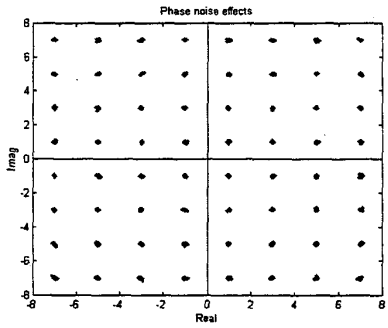

Figure 12 - 64 QAM phase rotation (CPE correction)

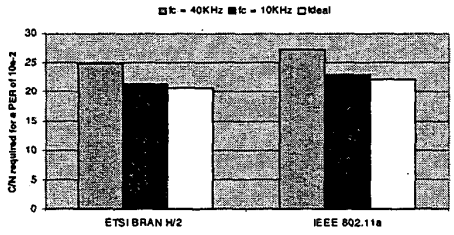

Figure 13 -Comparison of PER performance for Physical layer Mode 6 over channel E with uncorrected phase noise

Figure 13 shows the impact of phase noise on the PER performance. The simulations were performed for PHY bursts consisting of 10 Long Protocol Data Units (PDU) [13] in ETSI HiperLAN/2 and 1500 bytes for ETSI BRAN HiperLAN/2. This length was chosen to emphasise the effects of uncorrected phase noise. It is clear that as the corner frequency in the phase noise model increases we see greater degradation in overall performance. For a corner frequency of 100Hz (with the slope and noise floor quote previously), no significant degradation in performance was observed. Performance will worsen at higher slopes and phase noise floors. Hence the design of the oscillators should be seen as a vital component in the overall system design.

V. CONCLUSIONS

Robust time synchronisation was achieved via processing of the long double-symbol preamble. In channel model 'E' (representative of a worst case outdoor environment), positive time offsets were observed since the delay spread now leaks beyond the guard interval into the subsequent OFDM symbol. A performance degradation of less than 0.2 dB was observed due to the process of adaptive symbol timing recovery. Frequency offset correction showed favourable results with fine frequency estimates at very low values of MSE. Even in the presence of extremely long delay spreads (where fine frequency offset correction is reported to suffer), a maximum degradation of 1.8dB was seen relative to the ideal case. The presence of phase noise is expected to degrade the process of frequency offset estimation since this process relies heavily on the periodicity of the preamble time domain waveform and on maintaining identical subbands across the double-length SC structure. It is also shown that high frequency phase noise damages performance by introducing uncorrectable ICI into the OFDM waveform. The RF design should minimise high frequency phase noise this resulting in correctable CPE.

ACKNOWLEDGEMENTS

The authors would like to acknowledge the financial support of QinetiQ, the software modules and support of Mr Mike Butler and the useful insights provided by Dr Yusuf Baltaci.

REFERENCES

[1] Jan-Jaap van de Beek, Magnus Sandell and Per Ola Bŷrjesson, "ML Estimation of Time and Frequency Offset in OFDM Systems", *IEEE Transactions on Signal Processing*, vol. 45, no. 7, pp. 1800-1805, July 1997.

[2] J. Stott, "The Effects of Phase Noise in COFDM", EBU Technical Review, Summer 1998.

[3] ETSI, "Broadband Radio Access Networks (BRAN); HIPERLAN type 2 technical specifications; Physical (PHY) layer,". <DTS/BRAN-0023003> V0.k., August 1999.

[4] IEEE Std 802.11a/D7.0-1999, Part11: Wireless LAN Medium Access Control (MAC) and Physical Layer (PHY) specifications: High Speed Physical Layer in the 5GHz Band, 1999.

[5] <DTS/BRAN0020004-1> V0.m (1999-12), Broadband Radio Access Networks (BRAN); HIPERLAN TYPE 2; Data Link Control (DLC) Layer, Part 1: Basic Data Transport Function

[6] Paul H. Moose, "A Technique for Orthogonal Frequency Division Multiplexing Frequency Offset Correction", IEEE Transactions on Communications, vol. 42, no. 10, pp 2908-2913, October 1994.

[7] Vicenc Almenar, Saied Abedi and Rahim Tafazoli, 'Synchronization techniques for HIPERLAN/2', IEEE VTC Fall 2001.

[8] R. Van Nee and R. Prasad, "OFDM for Wireless Multimedia Communications", Artech House, 2000.

[9] T.M Schmidl and Donald Cox, "Robust Frequency and Timing Synchronization for OFDM", IEEE Transactions on Communications, vol. 45, no. 12, pp 1613-1621, December 1997.

[10] Joel Kirschman and Kurt Matis, "Modelling phase noise leads to lower BER in fixed wireless design", November 15, 2001. http://www.electronicengineering.com/features/comm/OEG20011114S0055

[11] John R. Pelliccio, Heinz Bachmann and Bruce W. Meyers, "Phase Noise Effects on OFDM Wireless LAN Performance", http://www.amwireless.com/archives/2001/v13n7/v13n7pg68.pdf

[12] Juha Heiskala and John Terry, "OFDM Wireless LANs: A Theoretical and Practical Guide", SAMS Publishing, 2002

[13] A. Doufexi, S. Armour, P. Karlsson, A.R. Nix, D. Bull, "Throughput Performance of WLANs Operating at 5 GHz Based on Link Simulations with Real and Statistical Channels", VTC'01 Spring, Rhodes, May 2001.